



Bayesian parameter estimation from dispersion relation observation data with Poisson processShun Katakami,^{1,2} Hirotaka Sakamoto,^{2,3} Kenji Nagata⁴,, Taka-hisa Arima,³ and Masato Okada^{1,3,*}¹*Graduate School of Science, The University of Tokyo, Tokyo 113-0033, Japan*²*Research Fellow of Japan Society for the Promotion of Science, Tokyo, Chiyoda 102-0083, Japan*³*Graduate School of Frontier Sciences, The University of Tokyo, Kashiwa, Chiba 277-8561, Japan*⁴*Research and Services Division of Materials Data and Integrated System, National Institute for Materials Science, 1-2-1 Sengen, Tsukuba, Ibaraki 305-0047, Japan*

(Received 27 July 2021; revised 5 April 2022; accepted 20 April 2022; published 6 June 2022)

In this study, we estimate the distribution of lattice model parameters based on Bayesian estimation using the dispersion relation spectral data of lattice vibration. The dispersion relation of lattice vibration is observed using inelastic scattering of neutrons or x rays and is used to analyze the speed of sound and interatomic force. However, the current analysis method of dispersion relation observation data in the field of experimental physics requires manually fitting parameters, so the analysis is costly and cannot effectively handle high-dimensional data and large amounts of data. Moreover, it is impossible to discuss the estimation accuracy with the conventional method. Therefore, we solve these problems by estimating the distribution of parameters using Bayesian inference. We propose a lattice model parameter estimation method that uses Bayesian inference with a physical observation stochastic process and determine the method's effectiveness using artificial data.

DOI: [10.1103/PhysRevE.105.065301](https://doi.org/10.1103/PhysRevE.105.065301)**I. INTRODUCTION**

In condensed-matter physics, various physical responses occur in terms of elementary excitations. Each elementary excitation is characterized by its energy (frequency) and momentum (wave vector). The energy and momentum are connected by a dispersion relation, which is one of the more important characteristics of elementary excitation. The dispersion relations are also essential to understanding sound propagation, specific heat, thermal conductivity, superconductivity, etc. Dispersion relations of bosonic excitations are generally observed by neutron scattering or x-ray scattering. The phonon dispersion relation was first observed in an inelastic neutron scattering measurement of germanium by Brockhouse and Iyengar [1,2]. Since then, the inelastic neutron scattering technique has been widely used for studying phonons. In the early days of inelastic neutron scattering, a reactor-based neutron source was utilized. The amount of obtained data was small and could be analyzed in a simple way irrelevant to the type of spectrometer. First, peak positions in the inelastic scattering spectrum at a certain momentum transfer \mathbf{q} were estimated and regarded as the eigenfrequencies of phonons. Then, the obtained dispersion relation was fitted to a theoretical model with variable parameters and the validity of the model was evaluated intuitively. The establishment of high-power accelerator-based neutron sources like ISIS, SNS, J-PARC, and CSNS and the combination of a high-power pulsed source and two-dimensional position-sensitive detectors remarkably improved data acquisition efficiency. A time-of-flight neutron spectrometer designed for inelas-

tic scattering measurements like MAPS [3], MERLIN [4], HYSPEC [5], ARCS [6], 4SEASONS [7], AMATERAS [8], and HRC [9] produces a large amount of event data in a four-dimensional (4D) frequency (ω)–momentum (\mathbf{q}) space that can be obtained within a couple of days. Analysis of event data is presently visualized as a two-dimensional contour plot of a one-dimensional spectrum for specified regions in the 4D space. Then, the physical model parameters are inferred to fit the estimated dispersion relations. However, the fitting is usually performed only for the visualized specified regions based on experience. Since the analysis is limited for the visualized data, it is impossible to effectively perform the inference of the physical parameters by considering all the event data.

To solve these problems, we propose a method of estimating the distribution of model parameters directly from high-dimensional event data. We estimate model parameters in the framework of Bayesian inference. In recent years, the estimation of model parameters by Bayesian inference has been actively applied to physical property research together with spectroscopy [10–15]. Since the calculation of Bayesian posterior probabilities is difficult theoretically, it is calculated numerically using the exchanged Markov chain Monte Carlo (REMC) method [16–19]. In a previous study [20], we assumed Gaussian noises in the observation process for the inference. The fluctuation of event numbers often follows the Poisson process. In this study, we improve the method of estimating the model parameter distributions by introducing Poisson noise into the observation process.

We conduct numerical experiments using a simple model and artificial data. The dispersion relations are calculated as the vibration eigenmodes of the classical harmonic-oscillator lattice model of the body-centered cubic type. We assume that each eigenmode is expressed as a Lorentzian with an identical

*okada@edu.k.u-tokyo.ac.jp

peak height and width as a function of energy. Some sets of artificial histogram data are generated from the Poisson process of the obtained spectral intensities. We show that our method is superior to the previous research method for data with a short observation time in terms of accuracy and reliability of Bayesian estimation.

II. FORMULATION OF DATA GENERATION PROCESS

In this study, we propose a method of estimating lattice parameters from the event data of a histogram. The analysis target is a body-centered cubic harmonic lattice model.

A. Dispersion relation

Let $\mathbf{u}(\mathbf{r}, t)$ be the displacement vector and let the variable a be the lattice constant. In addition, the elastic constants for the first, second, and third nearest neighbors are set to α_1 , α_2 , and α_3 , respectively. The eigenequation of motion is expressed as

$$-\omega^2 M \mathbf{u}(\mathbf{q}) = D \mathbf{u}(\mathbf{q}), \quad (1)$$

where $\mathbf{u}(\mathbf{q})$ is the Fourier transformation of the displacement vector

$$\mathbf{u}(\mathbf{r}, t) = \mathbf{u}(\mathbf{q}) e^{i(\mathbf{q}\cdot\mathbf{r} - \omega t)}, \quad (2)$$

M is the mass of the atom, and the coefficient matrix D is the q -dependent real symmetric matrix of 3×3 .

The diagonal component d_{ii} and the off-diagonal component d_{ij} of D are

$$\begin{aligned} d_{11} = & \frac{8}{3} \alpha_1 \left[\cos\left(\frac{aq_x}{2}\right) \cos\left(\frac{aq_y}{2}\right) \cos\left(\frac{aq_z}{2}\right) - 1 \right] \\ & + 2\alpha_2 [\cos(aq_x) - 1] \\ & + 2\alpha_3 \{\cos(aq_x) [\cos(aq_y) + \cos(aq_z)] - 2\}, \end{aligned} \quad (3)$$

$$\begin{aligned} d_{22} = & \frac{8}{3} \alpha_1 \left[\cos\left(\frac{aq_x}{2}\right) \cos\left(\frac{aq_y}{2}\right) \cos\left(\frac{aq_z}{2}\right) - 1 \right] \\ & + 2\alpha_2 [\cos(aq_y) - 1] \\ & + 2\alpha_3 \{\cos(aq_y) [\cos(aq_z) + \cos(aq_x)] - 2\}, \end{aligned} \quad (4)$$

$$\begin{aligned} d_{33} = & \frac{8}{3} \alpha_1 \left[\cos\left(\frac{aq_x}{2}\right) \cos\left(\frac{aq_y}{2}\right) \cos\left(\frac{aq_z}{2}\right) - 1 \right] \\ & + 2\alpha_2 [\cos(aq_z) - 1] \\ & + 2\alpha_3 \{\cos(aq_z) [\cos(aq_x) + \cos(aq_y)] - 2\}, \end{aligned} \quad (5)$$

$$\begin{aligned} d_{12} = & -\frac{8}{3} \alpha_1 \sin\left(\frac{aq_x}{2}\right) \sin\left(\frac{aq_y}{2}\right) \cos\left(\frac{aq_z}{2}\right) \\ & - 2\alpha_3 \sin(aq_x) \sin(aq_y), \end{aligned} \quad (6)$$

$$\begin{aligned} d_{23} = & -\frac{8}{3} \alpha_1 \sin\left(\frac{aq_y}{2}\right) \sin\left(\frac{aq_z}{2}\right) \cos\left(\frac{aq_x}{2}\right) \\ & - 2\alpha_3 \sin(aq_y) \sin(aq_z), \end{aligned} \quad (7)$$

$$\begin{aligned} d_{31} = & -\frac{8}{3} \alpha_1 \sin\left(\frac{aq_z}{2}\right) \sin\left(\frac{aq_x}{2}\right) \cos\left(\frac{aq_y}{2}\right) \\ & - 2\alpha_3 \sin(aq_z) \sin(aq_x). \end{aligned} \quad (8)$$

Here, $\lambda_1(\mathbf{q})$, $\lambda_2(\mathbf{q})$, and $\lambda_3(\mathbf{q})$ are three eigenvalues of the matrix D . The dispersion relation can be described as

$$\omega_i = \sqrt{-\frac{\lambda_i(\mathbf{q})}{M}} \quad (i = 1, 2, 3). \quad (9)$$

B. Data observation process

The dispersion relation is observed as 4D histogram data that includes statistical noises. In this section, we introduce the observation process into the dispersion relation.

Each eigenmode has a lifetime. Thus the spectrum profile is represented by a Lorentzian. The intensity for energy E_i and momentum \mathbf{q}_j can be written as

$$I(E_i, \mathbf{q}_j; \boldsymbol{\alpha}) = \sum_{k=1}^3 \eta_k(\mathbf{q}_j) \phi_k[E_i; \mathbf{q}_j, \boldsymbol{\alpha}, \gamma(\mathbf{q})], \quad (10)$$

$$\phi_k(E; \mathbf{q}, \boldsymbol{\alpha}, \gamma) \propto \frac{1}{\pi} \frac{\gamma^2}{[E - \hbar\omega_k(\mathbf{q}; \boldsymbol{\alpha})]^2 + \gamma^2}. \quad (11)$$

$\gamma_k(\mathbf{q})$ is the width of a Lorentzian; $\eta_k(\mathbf{q})$ is the intensity of each mode basis, which is determined by the measurement system, momentum q , temperature, etc. γ_k is also dependent on the momentum \mathbf{q} and temperature in general. $\Theta = \{\boldsymbol{\alpha}, \boldsymbol{\eta}, \boldsymbol{\gamma}\}$ are considered as model parameters and $\boldsymbol{\alpha} = \{\alpha_1, \alpha_2, \alpha_3\}$.

For simplicity purposes, we assume that γ_k and η_k are constants:

$$I(E_i, \mathbf{q}_j; \Theta) = \sum_{k=1}^3 \eta_k \phi_k(E_i; \mathbf{q}_j, \boldsymbol{\alpha}, \gamma_k). \quad (12)$$

The observed average of spectral intensities \bar{y}_{ij} for the observation time T is represented as

$$\bar{y}_{ij} = [I(E_i, \mathbf{q}_j; \Theta) + B]T. \quad (13)$$

If the observation process follows Poisson distribution, the acquired spectral data $Y = \{y_{ij}\}$ can be

$$P(y_{ij} | I(E_i, \mathbf{q}_j; \Theta)) = \frac{\bar{y}_{ij}^{y_{ij}} \exp(-\bar{y}_{ij})}{y_{ij}!}. \quad (14)$$

Here, we introduce a uniform background B independent of energy or momentum.

C. Previous study: Observation process of data

In a previous study [20], we assumed that the observation process followed a Gaussian distribution, so the acquired spectral data $Y = \{y_{ij}\}$ can be

$$P(y_{ij} | I(E_i, \mathbf{q}_j; \Theta)) = \mathcal{N}(I(E_i, \mathbf{q}_j; \Theta), \sigma_{\text{REMC}}^2), \quad (15)$$

where σ_{REMC} is the lower bound noise intensity for REMC. In this study, since it is generally impossible to know the noise intensity of data, we estimate noise [21] by giving the noise a lower bound.

III. ANALYSIS

Bayesian inference

In this section, we show a method of estimating model parameters by Bayesian inference from the obtained observation

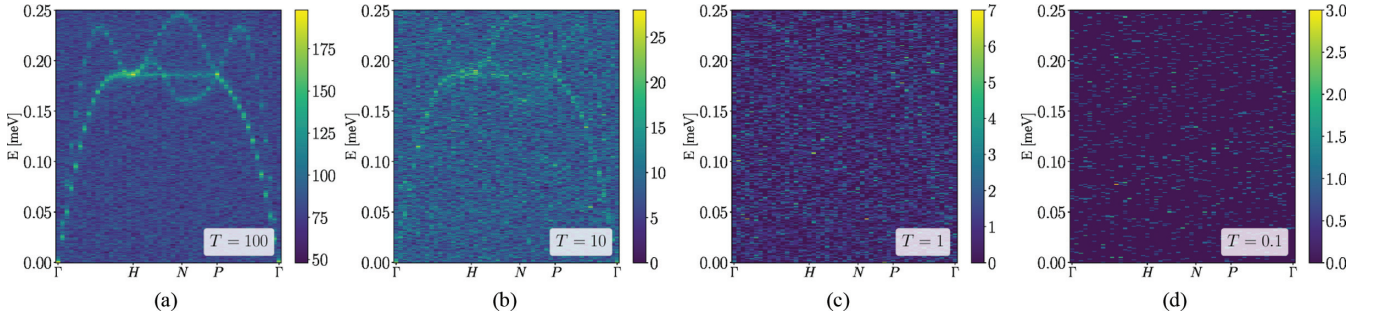


FIG. 1. Examples of the synthetic data of the generated dispersion relation. Panels (a)–(d) are spectrum data when $T = 100, 10, 1,$ and 0.1 , respectively. The parameters used to generate the data are shown in Table I.

data. The observation point is $X = \{x_{ij}|x_{ij} = (E_i, \mathbf{q}_j)\}$, and the observation value is $Y = \{y_{ij}\}$. We can write observation data $\mathcal{D} = \{X, Y\}$.

The amount of data is $N = |\mathcal{D}|$. Then, assuming that each observation follows the same independent distribution, the probability distribution of Y is

$$P(Y|X, \Theta) = \prod_{i,j} P(y_{ij}|I(E_i, \mathbf{q}_j; \Theta)), \quad (16)$$

$$= \prod_{i,j} \frac{\bar{y}_{ij}^{y_{ij}} \exp(-\bar{y}_{ij})}{y_{ij}!}, \quad (17)$$

$$= \exp[-N\mathcal{E}(\Theta)], \quad (18)$$

$$\mathcal{E}(\Theta) \equiv \frac{1}{N} \sum_{ij} (\bar{y}_{ij} - y_{ij} \ln \bar{y}_{ij} + \ln y_{ij}!). \quad (19)$$

From the Bayes' theorem, the posterior probability of the model parameter Θ is

$$P(\Theta|\mathcal{D}) = \frac{P(Y|X, \Theta)\varphi(\Theta)}{P(Y|X)}, \quad (20)$$

$$= \frac{1}{P(Y|X)} \varphi(\Theta) \prod_{i,j} P(y_{ij}|I(E_i, \mathbf{q}_j; \Theta)), \quad (21)$$

$$= \frac{1}{Z(\mathcal{D})} \exp(-N\mathcal{E})\varphi(\Theta), \quad (22)$$

where $\varphi(\Theta)$ is the prior distribution and $Z(\mathcal{D})$ is the marginal likelihood or normalization constant

$$Z(\mathcal{D}) = \int \exp[-N\mathcal{E}(\Theta)]\varphi(\Theta)d\Theta. \quad (23)$$

We use the prior distributions $\varphi(\Theta) = \varphi_\alpha(\boldsymbol{\alpha})\varphi_\gamma(\boldsymbol{\gamma})\varphi_\eta(\boldsymbol{\eta})$. Each distribution is written as half-Cauchy distributions $\varphi_\alpha(\boldsymbol{\alpha}) = \prod_{k=1}^3 C(\alpha_k; \iota_\alpha)$ and $\varphi_\eta(\boldsymbol{\eta}) = \prod_{k=1}^3 C(\eta_k; \iota_\eta)$ and the inverse gamma distribution $\varphi_\gamma(\boldsymbol{\gamma}) = \prod_{k=1}^3 G(\gamma_k; a_\gamma, b_\gamma)$, where the half-Cauchy distribution is

$$C(\eta; \iota_\eta) = \begin{cases} \frac{1}{\pi} \frac{\iota_\eta}{\eta^2 + \iota_\eta^2} & (\eta \geq 0), \\ 0 & (\eta < 0), \end{cases} \quad (24)$$

and the inverse gamma distribution is

$$G(\gamma; a_\gamma, b_\gamma) = \prod_i \frac{b_\gamma^{a_\gamma}}{\Gamma(a_\gamma)} \gamma_i^{-(a_\gamma+1)} e^{-b_\gamma/\gamma_i}. \quad (25)$$

These prior distributions are the same as those in the previous study [20].

In this study, the posterior probability distribution is calculated numerically by using the REMC method [16,22].

IV. NUMERICAL EXPERIMENT

In this section, we evaluate the performance of our model parameter estimation method that uses Bayesian inference. We show numerical experiments that compare the performances of our method and the previous method using the same synthetic data.

First, we generated the dispersion relation data of the body-centered cubic lattice model based on Eq. (14). The parameters used to generate the synthetic data are shown in Table I. We chose points with high symmetry in the first Brillouin zone of momentum space and sampled the straight line connecting each point $\Gamma[0, 0, 0] \rightarrow H[0, 0, 2\pi/a] \rightarrow N[0, \pi/a, \pi/a] \rightarrow P[\pi/a, \pi/a, \pi/a] \rightarrow \Gamma[0, 0, 0]$.

Examples of the synthetic data are shown in Fig. 1. Figures 1(a)–1(d) are the spectrum data when the observation time is $T = 100, 10, 1, 0.1$. Model parameter estimation is obtained as a posterior probability of the spring constant sampled by the REMC method (see Table II).

Figures 2–5 show examples of spring constant estimations. The posterior probability distributions for the synthetic data with observation time $T = 100, 10, 1, 0.1$ [Figs. 1(a)–1(d)] are Figs. 2–5.

The estimated mean and the spread of the estimated distribution are shown statistically because the spread of the distribution was evaluated as the reliability in our numerical experiments. For simplicity purposes, we consider the standard deviation as the spread of the estimated distribution. To statistically evaluate the mean and standard deviation obtained

TABLE I. Parameters of synthetic data. (Note that the phonon energy is independent of the lattice constant a . The lattice constant is relevant only to the size of the first Brillouin zone.)

N	50
$(\alpha_1, \alpha_2, \alpha_3)$ (N/m)	(300, 200, 100)
(η_1, η_2, η_3)	(1, 1, 1)
$(\gamma_1, \gamma_2, \gamma_3)$ (meV)	(0.0025, 0.0025, 0.0025)
M_{atom} (kg)	2×10^{-26}
B	0.8

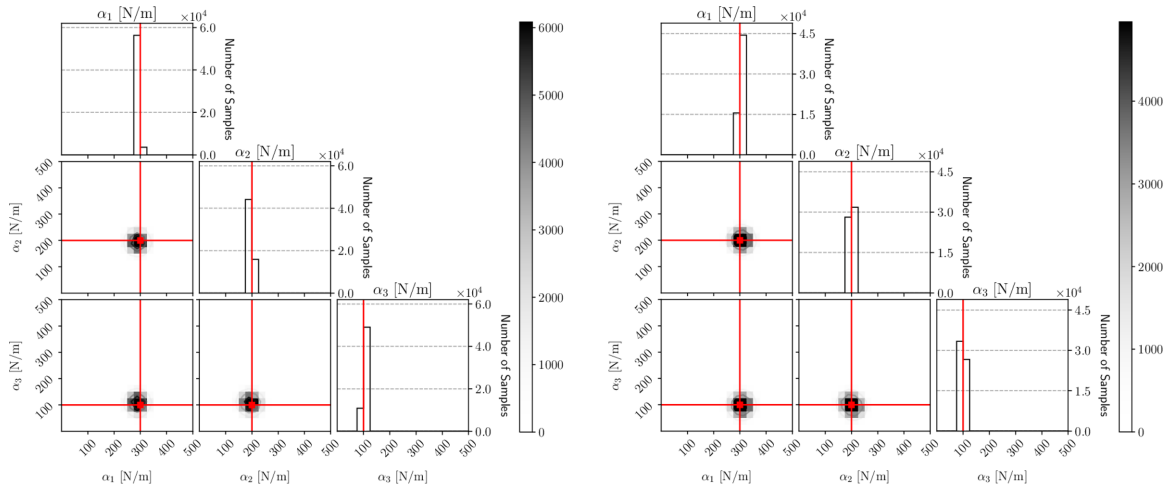


FIG. 2. Posterior distributions of α for the observation data generated by $T = 100$. The results with the proposed and previous method are shown on the left and right, respectively. The intersections of the red lines represent the true α . The parameters used for the REMC method of estimating α are shown in Table I.

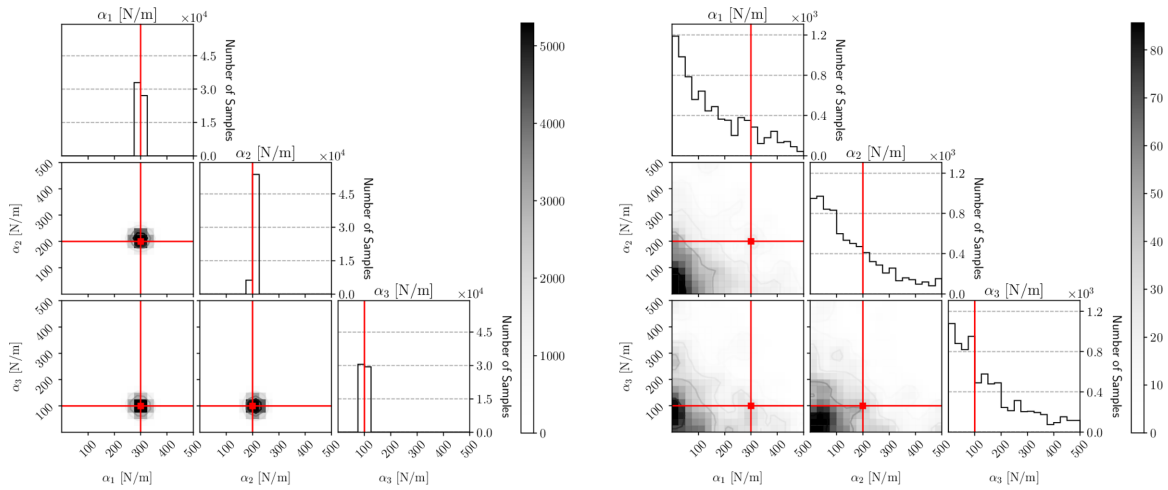


FIG. 3. Posterior distributions of α for the observation data generated by $T = 10$. The results with the proposed and previous method are shown on the left and right, respectively. The intersections of the red lines represent the true α . The parameters used for the REMC method of estimating α are shown in Table I.

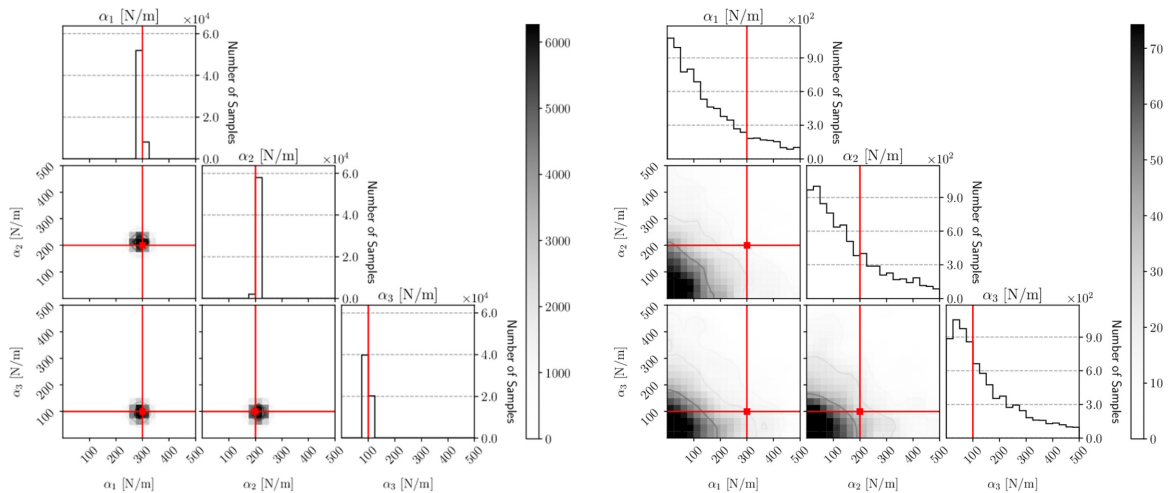


FIG. 4. Posterior distributions of α for the observation data generated by $T = 1$. The results with the proposed and previous method are shown on the left and right, respectively. The intersections of the red lines represent the true α . The parameters used for the REMC method of estimating α are shown in Table I.

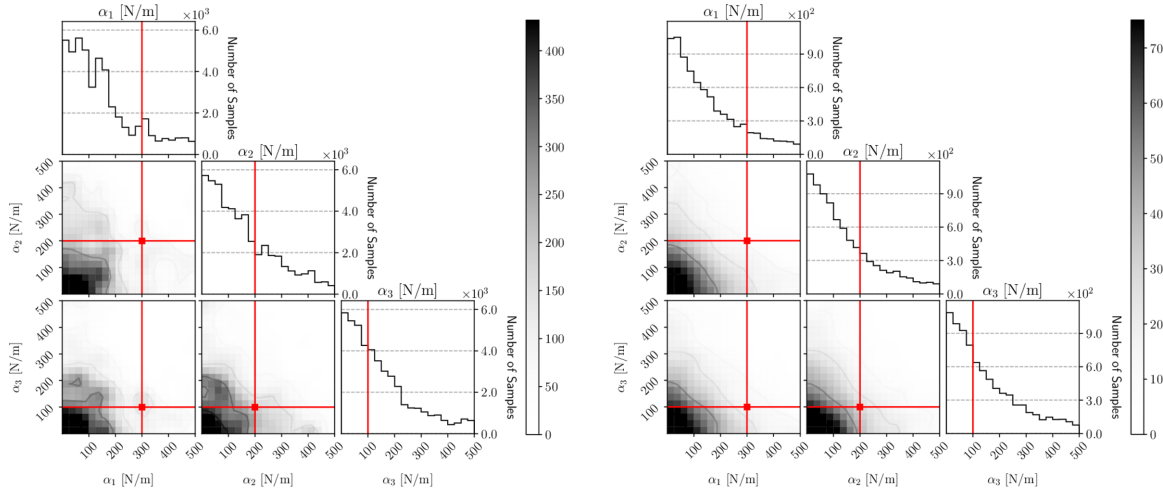


FIG. 5. Posterior distributions of α for the observation data generated by $T = 0.1$. The results with the proposed and previous method are shown on the left and right, respectively. The intersections of the red lines represent the true α . The parameters used for the REMC method of estimating α are shown in Table I.

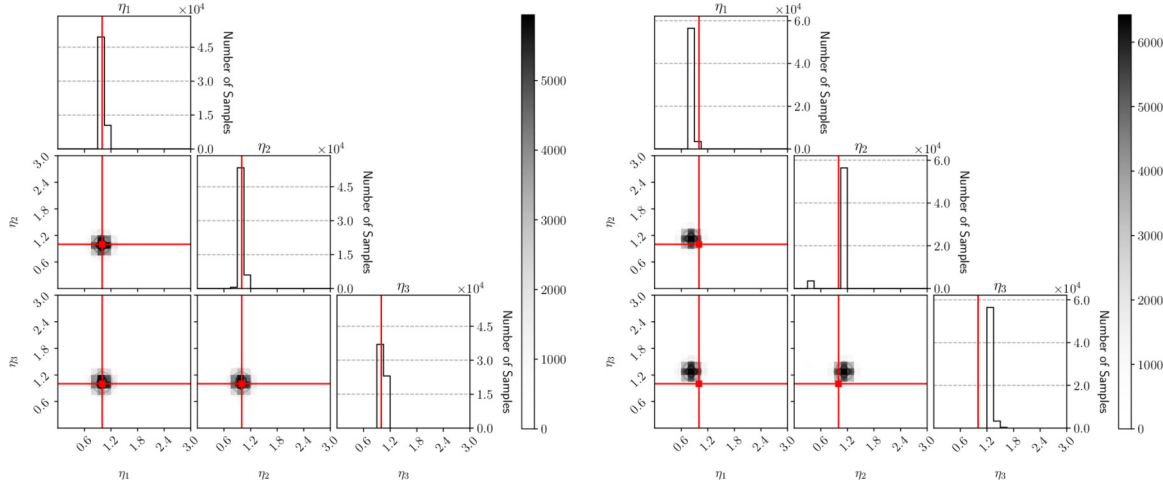


FIG. 6. Posterior distributions of η for the observation data generated by $T = 100$. The results with the proposed and previous method are shown on the left and right, respectively. The intersections of the red lines represent the true η . The parameters used for the REMC method of estimating η are shown in Table I.

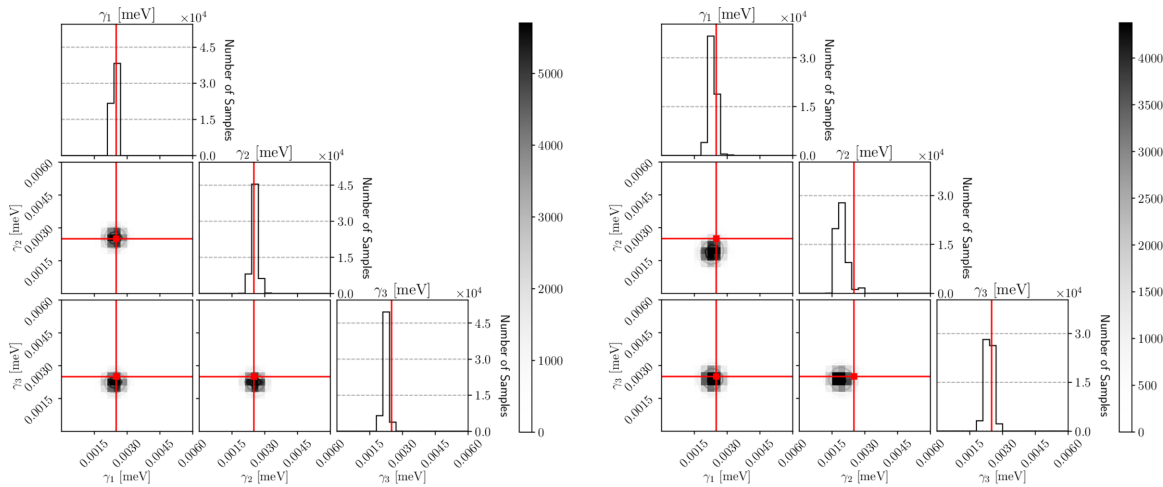


FIG. 7. Posterior distributions of γ for the observation data generated by $T = 100$. The results with the proposed and previous method are shown on the left and right, respectively. The intersections of the red lines represent the true γ . The parameters used for the REMC method of estimating γ are shown in Table I.

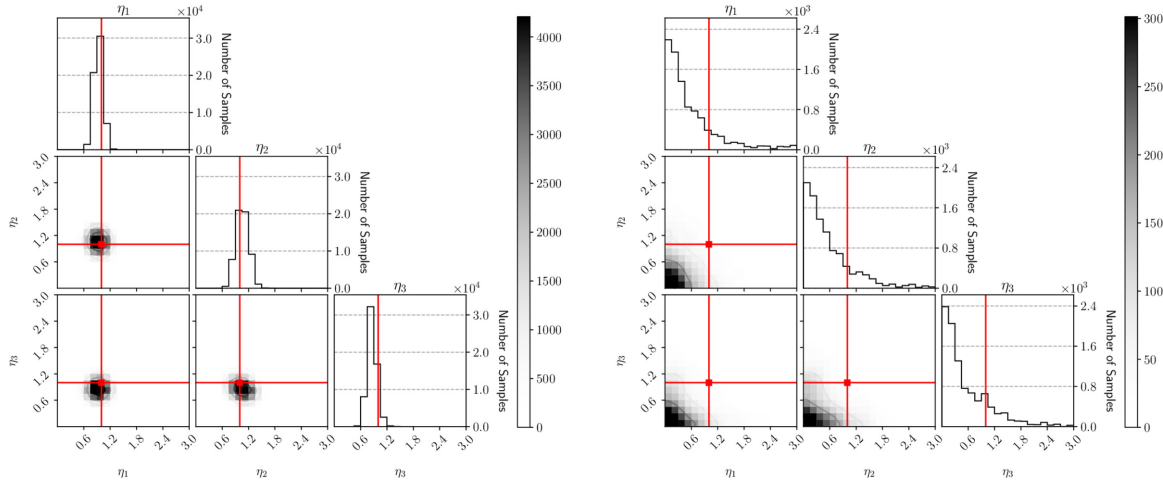


FIG. 8. Posterior distributions of η for the observation data generated by $T = 10$. The results with the proposed and previous method are shown on the left and right, respectively. The intersections of the red lines represent the true η . The parameters used for the REMC method of estimating η are shown in Table I.

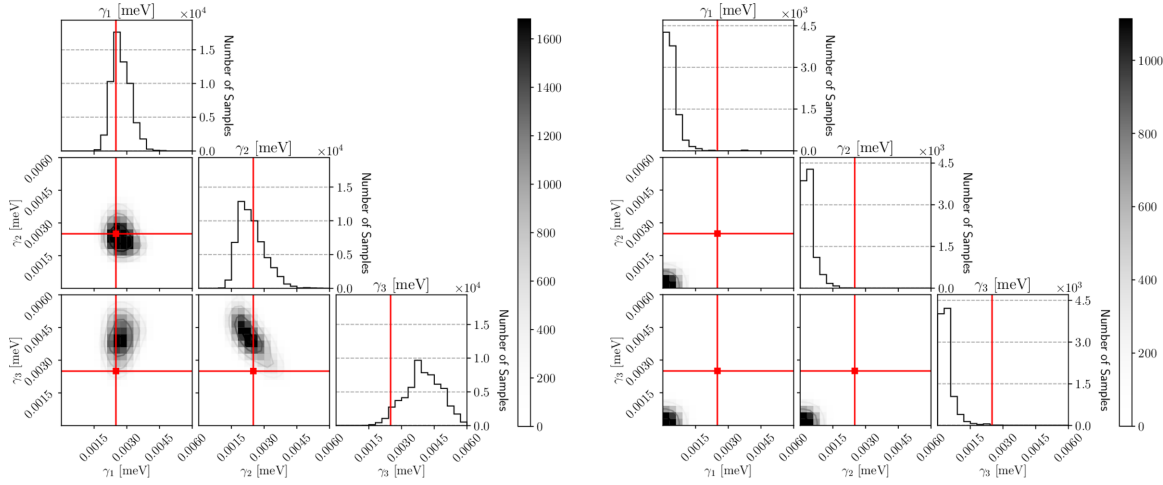


FIG. 9. Posterior distributions of γ for the observation data generated by $T = 10$. The results with the proposed and previous method are shown on the left and right, respectively. The intersections of the red lines represent the true γ . The parameters used for the REMC method of estimating γ are shown in Table I.

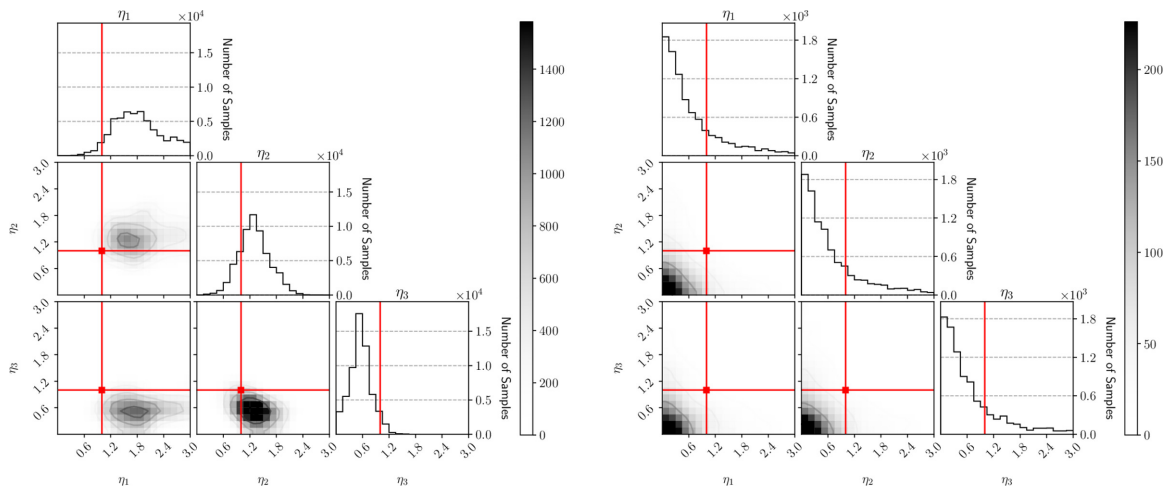


FIG. 10. Posterior distributions of η for the observation data generated by $T = 1$. The results with the proposed and previous method are shown on the left and right, respectively. The intersections of the red lines represent the true η . The parameters used for the REMC method of estimating η are shown in Table I.

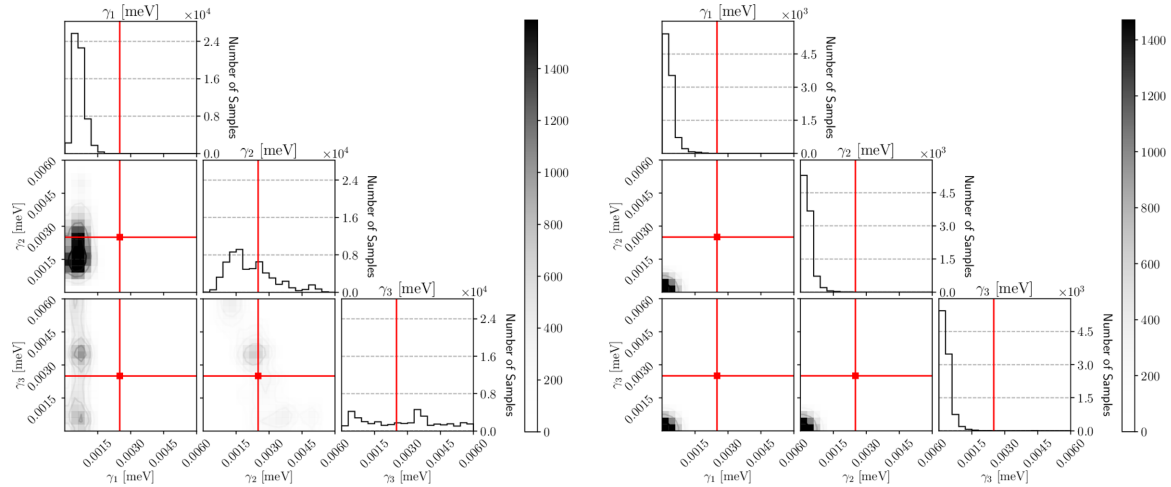


FIG. 11. Posterior distributions of γ for the observation data generated by $T = 1$. The results with the proposed and previous method are shown on the left and right, respectively. The intersections of the red lines represent the true γ . The parameters used for the REMC method of estimating γ are shown in Table I.

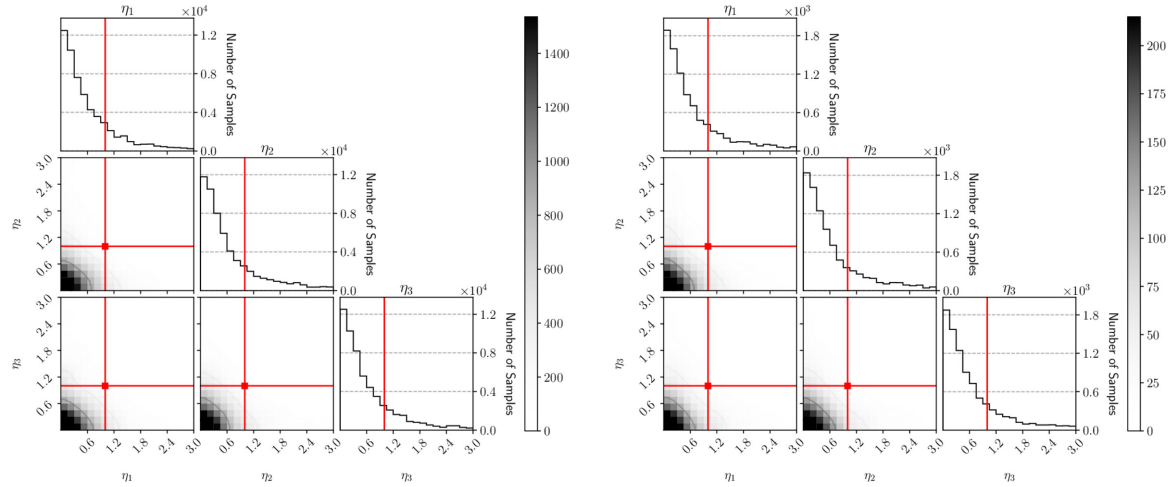


FIG. 12. Posterior distributions of η for the observation data generated by $T = 0.1$. The results with the proposed and previous method are shown on the left and right, respectively. The intersections of the red lines represent the true η . The parameters used for the REMC method of estimating η are shown in Table I.

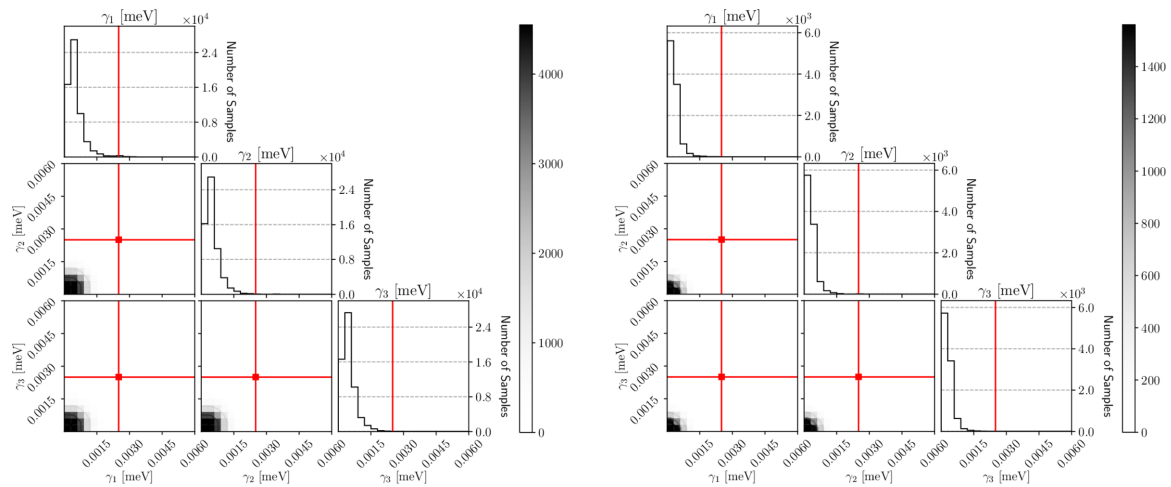


FIG. 13. Posterior distributions of γ for the observation data generated by $T = 0.1$. The results with the proposed and previous method are shown on the left and right, respectively. The intersections of the red lines represent the true γ . The parameters used for the REMC method of estimating γ are shown in Table I.

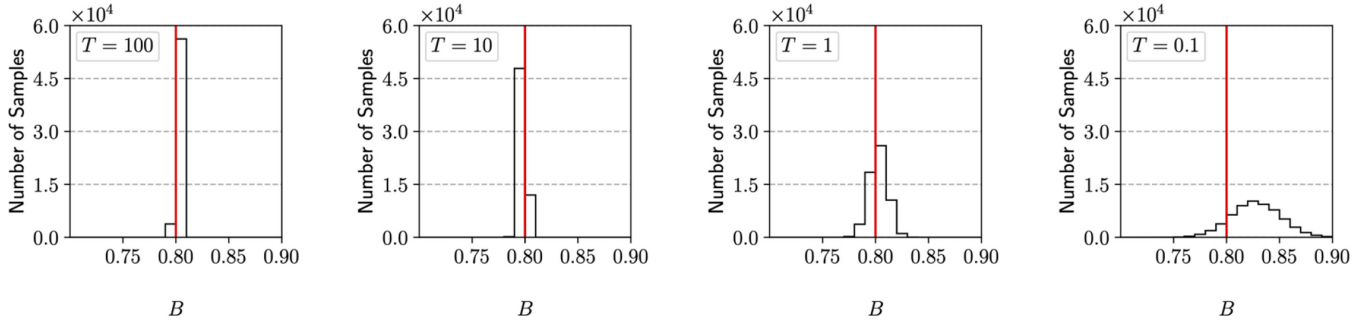


FIG. 14. Posterior distributions of B for the observation data generated by $T = 100, 10, 1, 0.1$. The parameters used for the REMC method of estimating B are shown in Table I. Note that the parameter B is fixed to the true value in the previous method [20].

by each inference, Tables III and IV show the average values and the standard deviations obtained with 10 inferences.

V. DISCUSSION

In the numerical experiments in Sec. IV, we compared the method proposed in this study with a method from a previous study and evaluated their performances in estimating physical model parameters from dispersion relation observation data. Since the observation data should be physical event measurement data, it was generated by the Poisson process.

Figures 2–5 show that our method was more accurate than the previous study’s method. In addition, Tables III and IV show that our method improved the inference performance by about 100 times with respect to the observation time compared with the previous study’s method.

The inference performance differed based on whether the model and the likelihood function matched. The likelihood function of the model of our method has a Poisson distribution, and the model and the generation process of observation data match. However, the likelihood function of the model of the previous study’s method has a Gaussian distribution, which does not match the generation process of the observation data. We determined that the estimation performance could be substantially reduced because the noise model of the estimation model did not match the noise mechanism of the observed data. An appropriate noise mechanism must be introduced into the estimation model to improve the estimation performance.

We constructed a model for inelastic scattering of the experimental data of neutrons, and we introduced the Poisson noise model since the acquired data was stochastically measured count data. Poisson noise can be used for the count

data of stochastic events. In the Poisson distribution, the mean and the variance are the same value, but there are actual data cases in which the mean and the variance of the distribution are not the same value even for count data. This is because there are noise factors that cannot be expressed by the Poisson distribution alone, such as the characteristics of measuring instruments or physical phenomena from other systems. In actual operation, if multiple noise models are possible, the noise model must be evaluated by model selection. In Bayesian inference, the appropriateness of the estimation model for the data can be measured using Bayesian free energy. First, the free energy is calculated for each model and the model with the minimum free energy is considered the most suitable model for the data.

Unlike the previous study’s method, it is not necessary to estimate the noise level in our method because it does not include noise parameters in the observation model. Therefore, the uncertainty due to noise estimation does not affect the parameter estimation and stable analysis results can be obtained by our method.

In event measurement, the data is better retained as raw count data. In the fields of physical measurement and information measurement, measurement data is often processed and not retained as raw count data. Our method dramatically improves estimation accuracy by being probabilistically modeled using a Poisson process on Bayesian inference and by treating the data as raw count data. The properties of count data can improve estimation accuracy. Therefore, in event measurement, the data should be retained as raw count data.

VI. CONCLUSION

We proposed a method of estimating the interaction parameters of the crystal lattice from dispersion relation observation data, conducted numerical experiments using artificial data, and discussed performance evaluations. We introduced the Poisson process into the inference model with our method. Therefore, our method achieved better inference accuracy than the previous study’s method and we could infer physical parameters with high accuracy from short-time measurement data. In future study, we will perform more practical Bayesian modeling for actual data analysis. The shell model [23] can be handled as a more practical model for calculating the dispersion relation of lattice vibration. By extending our model, we can achieve more accurate model parameter estimation and optimization of experimental observation conditions.

TABLE II. Parameters of the priors and REMC conditions for parameter estimation.

L	48
M	120 000
Burn in step	60 000
ι_α	150
ι_η	0.5
a_γ	4.001
b_γ (meV)	0.010 01
ξ	1.4

TABLE III. Descriptive statistics values of posteriors by Poisson EMC.

Time	Posterior mean			Posterior standard deviation		
	α_1 (N/m)	α_2 (N/m)	α_3 (N/m)	α_1 (N/m)	α_2 (N/m)	α_3 (N/m)
1000	300.00 ± 0.11	200.01 ± 0.09	100.03 ± 0.07	0.09 ± 0.00	0.11 ± 0.01	0.08 ± 0.01
100	299.93 ± 0.26	199.92 ± 0.40	100.07 ± 0.26	0.26 ± 0.01	0.33 ± 0.01	0.24 ± 0.02
10	300.33 ± 1.02	199.88 ± 1.05	99.69 ± 0.46	0.85 ± 0.09	1.10 ± 0.11	0.81 ± 0.08
1	301.72 ± 3.04	200.41 ± 4.46	98.65 ± 2.70	3.30 ± 1.39	3.67 ± 0.99	2.69 ± 0.96
0.1	1101.65 ± 924.92	1219.80 ± 2014.31	1056.90 ± 814.90	$12\ 382.66 \pm 15\ 656.31$	$9369.42 \pm 19\ 538.85$	$9769.06 \pm 12\ 901.07$

ACKNOWLEDGMENTS

This work was partly supported by KAKENHI Grant-in-Aid for Scientific Research (A) (Grant No. 18H04106), Grant-in-Aid for JSPS Research Fellows (Grant No. JP18J21951), and JST CREST (Grant No. JPMJCR1761).

APPENDIX: ESTIMATION RESULTS OF THE SPECTRUM PARAMETERS

Here, the estimation results of the other parameters of the proposed method in Sec. IV are described in Figs. 6–14.

TABLE IV. Descriptive statistics values of posteriors by Gaussian EMC.

Time	Posterior mean			Posterior standard deviation		
	α_1 (N/m)	α_2 (N/m)	α_3 (N/m)	α_1 (N/m)	α_2 (N/m)	α_3 (N/m)
1000	300.00 ± 0.06	199.99 ± 0.06	100.01 ± 0.03	0.08 ± 0.00	0.10 ± 0.00	0.07 ± 0.00
100	299.88 ± 0.39	199.98 ± 0.63	100.09 ± 0.35	0.89 ± 0.42	1.24 ± 0.40	0.95 ± 0.32
10	2869.40 ± 4335.94	1288.29 ± 685.08	1037.25 ± 327.82	$75\ 030.23 \pm 182\ 473.8$	$18\ 510.97 \pm 19\ 274.41$	$10\ 078.06 \pm 8481.60$
1	1092.83 ± 793.79	1469.85 ± 1518.43	973.71 ± 344.36	$28\ 949.34 \pm 54\ 884.65$	$41\ 824.27 \pm 78\ 722.12$	$18\ 154.27 \pm 26\ 247.32$
0.1	4154.65 ± 9067.73	1409.29 ± 1107.07	1061.90 ± 235.39	$325\ 395.19 \pm 898\ 216.3$	$45\ 478.45 \pm 74\ 316.54$	$24\ 386.52 \pm 17\ 130.80$

- [1] B. N. Brockhouse and P. K. Iyengar, Normal vibrations of germanium by neutron spectrometry, *Phys. Rev.* **108**, 894 (1957).
- [2] B. N. Brockhouse and P. K. Iyengar, Normal modes of germanium by neutron spectrometry, *Phys. Rev.* **111**, 747 (1958).
- [3] T. Perring, A. Taylor, R. Osborn, D. Paul, A. Boothroyd, and G. Aeppli, Maps: A chopper spectrometer to measure high energy magnetic excitations in single crystals, in *Proceedings of the 12th Meeting of the Collaboration on Advanced Neutron Sources (ICANS-XII)*, 1994, Vol. I (unpublished).
- [4] R. Bewley, R. Eccleston, K. McEwen, S. Hayden, M. Dove, S. Bennington, J. Treadgold, and R. Coleman, Merlin, a new high count rate spectrometer at isis, *Phys. B: Condens. Matter* **385–386**, 1029 (2006).
- [5] B. Winn, U. Filges, V. Garlea, M. Graves-Brook, C. J. M. Hagen, M. Kenzelmann, L. Passell, S. Shapiro, X. Tong, and I. Zaliznyak, Recent progress on hyspec, and its polarization analysis capabilities, *EPJ Web Conf.* **83**, 0301 (2015).
- [6] D. Abernathy, M. Stone, M. Loguillo, M. Lucas, O. Delaire, X. Tang, J. Lin, and B. Fultz, Design and operation of the wide angular-range chopper spectrometer arcs at the spallation neutron source, *Rev. Sci. Instrum.* **83**, 015111 (2012).
- [7] M. Nakamura, R. Kajimoto, Y. Inamura, F. Mizuno, M. Fujita, T. Yokoo, and M. Arai, First demonstration of novel method for inelastic neutron scattering measurement utilizing multiple incident energies, *J. Phys. Soc. Jpn.* **78**, 093002 (2009).
- [8] K. Nakajima, S. Ohira-Kawamura, T. Kikuchi, M. Nakamura, R. Kajimoto, Y. Inamura, N. Takahashi, K. Aizawa, K. Suzuya, K. Shibata *et al.*, Amateras: A cold-neutron disk chopper spectrometer, *J. Phys. Soc. Jpn.* **80**, SB028 (2011).
- [9] S. Itoh, T. Yokoo, S. Satoh, S.-I. Yano, D. Kawana, J. Suzuki, and T. J. Sato, High resolution chopper spectrometer (hrc) at j-parc, *Nucl. Instrum. Methods Phys. Res. A* **631**, 90 (2011).
- [10] Y.-i. Mototake, M. Mizumaki, I. Akai, and M. Okada, Bayesian Hamiltonian selection in x-ray photoelectron spectroscopy, *J. Phys. Soc. Jpn.* **88**, 034004 (2019).
- [11] K. Iwamitsu, M. Okada, and I. Akai, Bayesian spectroscopy with a replica exchange Monte Carlo method on an excitonic absorption spectrum of a Cu2O thin crystal, *J. Phys.: Conf. Ser.* **1220**, 012009 (2019).
- [12] K. Iwamitsu, T. Yokota, K. Murata, M. Kamezaki, M. Mizumaki, T. Uruga, and I. Akai, Spectral analysis of x-ray absorption near edge structure in α -Fe2O3 based on Bayesian spectroscopy, *Phys. Status Solidi B* **257**, 2000107 (2020).
- [13] K. Iwamitsu, M. Okada, and I. Akai, Spectral decomposition of components weaker than noise intensity by Bayesian spectroscopy, *J. Phys. Soc. Jpn.* **89**, 104004 (2020).
- [14] T. Yamasaki, K. Iwamitsu, H. Kumazoe, M. Okada, M. Mizumaki, and I. Akai, Bayesian spectroscopy of synthesized soft x-ray absorption spectra showing magnetic circular dichroism at the Ni-L3,-L2 edges, *Sci. Technol. Adv. Mater.: Methods* **1**, 75 (2021).
- [15] Y. Yokoyama, N. Tsuji, I. Akai, K. Nagata, M. Okada, and M. Mizumaki, Bayesian orbital decomposition and determination

- of end condition for magnetic compton scattering, *J. Phys. Soc. Jpn.* **90**, 094802 (2021).
- [16] K. Hukushima and K. Nemoto, Exchange Monte Carlo method and application to spin glass simulations, *J. Phys. Soc. Jpn.* **65**, 1604 (1996).
- [17] K. Nagata, R. Muraoka, Y.-I. Mototake, T. Sasaki, and M. Okada, Bayesian spectral deconvolution based on Poisson distribution: Bayesian measurement and virtual measurement analytics (vma), *J. Phys. Soc. Jpn.* **88**, 044003 (2019).
- [18] K. Okajima, K. Nagata, and M. Okada, Fast Bayesian deconvolution using simple reversible jump moves, *J. Phys. Soc. Jpn.* **90**, 034001 (2021).
- [19] K. Iwamitsu, Y. Nishi, T. Yamasaki, M. Kamezaki, K. Higashiyama, S. Yakura, H. Kumazoe, S. Aihara, K. Nagata, M. Okada *et al.*, Replica-exchange Monte Carlo method incorporating auto-tuning algorithm based on acceptance ratios for effective Bayesian spectroscopy, *J. Phys. Soc. Jpn.* **90**, 104004 (2021).
- [20] H. Sakamoto, S. Katakami, K. Muto, K. Nagata, T.-H. Arima, and M. Okada, Bayesian parameter estimation using dispersion relation spectra, *J. Phys. Soc. Jpn.* **89**, 124002 (2020).
- [21] S. Tokuda, K. Nagata, and M. Okada, Simultaneous estimation of noise variance and number of peaks in Bayesian spectral deconvolution, *J. Phys. Soc. Jpn.* **86**, 024001 (2016).
- [22] K. Nagata and S. Watanabe, Exchange Monte Carlo sampling from Bayesian posterior for singular learning machines, *IEEE Trans. Neural Networks* **19**, 1253 (2008).
- [23] R. A. Cowley, W. Cochran, B. N. Brockhouse, and A. D. B. Woods, Lattice dynamics of alkali halide crystals. III. Theoretical, *Phys. Rev.* **131**, 1030 (1963).